Rashtbari et al., *BioImpacts.* 2024;14(5):29946
doi: 10.34172/bi.2024.29946
https://bi.tbzmed.ac.ir/

The effects of Fe_2O_3 nanoparticles on catalytic function of human acetylcholinesterase: size and concentration role

Samaneh Rashtbari[#], Zahra Hassanpour Aydinlou[#], Leila Sadeghi[*]

Department of Animal Biology, Faculty of Natural Science, University of Tabriz, Tabriz, Iran
[#]Samaneh Rashtbari and Zahra Hassanpour Aydinlou are equal contributors to this work and designated as co-first authors.

Article Info

Article Type:
Original Article

Article History:
Received: 10 Jun. 2023
Revised: 12 Oct. 2023
Accepted: 24 Oct. 2023
ePublished: 5 Feb. 2024

Keywords:
Acetylcholinesterase, Fe_2O_3 nanoparticles, Fluorescence spectroscopy, Circular dichroism

Abstract

Introduction: Fe_2O_3 NPs can enter cells quickly, pass through the blood-brain barrier and interact with macromolecules. These materials are widely used in different fields, so their risk assessment is among the most critical issues. Acetylcholinesterase (AChE) is a cholinergic enzyme in central and peripheral nervous systems.

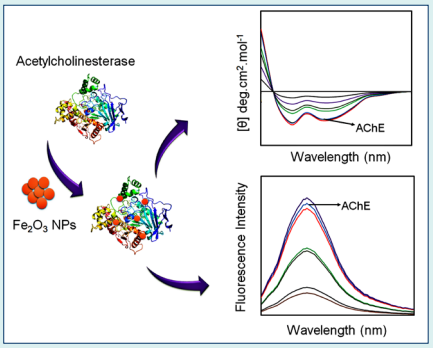

Methods: In this work, the possible effects of Fe_2O_3 NPs on the structure and catalytic activity of AChE were investigated using circular dichroism (CD), surface plasmon resonance (SPR), and fluorescence spectroscopies.

Results: The outcomes demonstrated that 5 nm Fe_2O_3 NPs inhibit AChE activity through mixed mechanism. While 50 nm Fe_2O_3 NPs caused an enhancement in the catalytic activity up to 60 nM. However, higher concentrations of Fe_2O_3 NPs (above 60 nM) hindered the enzyme activity via mixed mechanism. Fluorescence analysis showed that NPs can quench the fluorescence intensity of AChE that refer to conformational changes. Furthermore, CD results showed that Fe_2O_3 NPs can reduce the α-helix and β-sheet contents of the enzyme and decrease the stability of AChE. Also, the SPR data analysis showed that the affinity between AChE and Fe_2O_3 NPs decreased with rising temperature. After treatment with Fe_2O_3 NPs, the catalytic activity of AChE was assessed in HepG2 cell lines, and the results confirmed the inhibitory effects of Fe_2O_3 NPs on AChE activity *in vivo*.

Conclusion: These findings provide helpful information about the impact of Fe_2O_3 NPs on the structure and function of AChE and could offer new insights into the risk assessment of the medical application of nanoparticles.

Introduction

In recent years, the use of various nanoparticles (NPs) has expanded widely in different areas, including medicine, engineering, catalysis, and environmental remediation.[1] This is due to the unique properties of these materials, such as their electrical, optical, chemical, magnetic, and magneto-optical properties.[2-4] Given the widespread use of NPs, risk assessment of these materials is critical, and their toxicity has become one of the main challenges among researchers. So far, different kinds of NPs have been synthesized and developed. Iron oxide NPs (which consist of maghemite (γ-Fe_2O_3) and/or magnetite (Fe_3O_4) particles) are among the most important nanomaterials.[5]

Fe_2O_3 NPs have gained considerable attention because of their unique intrinsic features, such as outstanding biocompatibility and superior magnetic properties.[6,7] These NPs are widely used in a variety of fields, such as sensing technologies, memory storage devices, magnetic separation, magnetic labeling, catalytic processes, and biomedicine (heating for hyperthermia treatments, providing contrast effects for magnetic imaging, and remotely controlling the delivery of targeted drugs).[8-10]

NPs are small particles with large surface-to-volume ratios.[11,12] It has been accepted that the small size of NPs can cause these materials to enter cells quickly, pass through the blood-brain barrier, and interact with different kinds of proteins and enzymes.[13] In general, the conformation and function of enzymes and proteins are widely associated with their tertiary structure and protein dysfunction can lead to various diseases and disorders.[14]

*Corresponding author: Leila Sadeghi, Email: l.sadeghi@tabrizu.ac.ir and l.sadeghi66@yahoo.com

Acetylcholinesterase (AChE), a critical serine hydrolase, is secreted into the synaptic space by postsynaptic cholinergic neurons.[15] AChE is a crucial enzyme for the growth and operation of the central nervous system. This enzyme also has a significant impact on neurodevelopment and hematological differentiation.[16,17] In the synaptic space, it promotes the breakdown of acetylcholine into choline and acetate.[18] According to studies, the inhibition of AChE leads to an accumulation of acetylcholine in the synaptic cleft. It disrupts the neurotransmitter levels in the synapses, which overexcites nicotinic and muscarinic acetylcholine receptors and impairs neurotransmission.[19,20]

According to the previous experiment, Fe_2O_3 NPs could change brain proteome and affect the cholinergic function of a rat's brain.[21] Therefore, the main objective of the present work was to investigate the possible effects of Fe_2O_3 NPs on the structure and catalytic activity of AChE via spectroscopic methods. On the other hand, the activity of AChE extracted from HepG2 cell lines was evaluated after exposure to Fe_2O_3 NPs with two different sizes (5 and 50 nm).

Materials and Methods

Materials

Human acetylcholinesterase enzyme (AChE), 5,5'-dithio-bis-(2-nitrobenzoic) acid (DTNB), acetylthiocholine iodide ethanaminium, and Fe_2O_3 NPs (Fe_2O_4 NPs; with the size of 5 and 50 nm), N-ethyl-N-(3-dimethyl aminopropyl) carbodiimide (EDC), N-hydroxysuccinimide (NHS), NaCl, and NaOH were provided from Sigma Aldrich Company (St. Louis, MO, USA).

Methods

Preparation and characterization of NPs

Fe_2O_3 NPs were prepared from Sigma-Aldrich Company and dispersed by sonication (10 min, 750 W, and 20 kHz) in phosphate buffer (pH 7) before use. Size distribution and NPs dispersion were evaluated by the dynamic light scattering (DLS) and TEM methods. Fig. 1 shows Fe_2O_3 NP in crystalline phase with 5 and 50 nm sizes. In this work, the high-purity Fe_2O_3 NPs (99%) were used without coating. The prepared particles had γ-Fe_2O_3 crystalline phase with spherical morphology. Also, the specific surface areas of Fe_2O_3 NP with 5 nm and 50 nm were 450–2000 m^2/g and 50–245 m2/g, respectively.

AChE activity assay

The catalytic activity of AChE in the presence of Fe_2O_3 NP was investigated using Ellman's colorimetric method.[22] For this purpose, additional concentrations of Fe_2O_3 NP (0-2500 nM) were added to the reaction solution containing phosphate buffer (0.1 M, pH 7.0) and AChE (0.7 µg/mL). After incubating for 2 hours, DTNB and acetylcholine iodide (as a substrate) were added to the mixture. DTNB and substrate had final concentrations of 0.33 mM and 1.56 mM, respectively. Following incubation of the prepared reaction mixture for 5.0 minutes at 25 °C, the rate of acetylcholine iodide hydrolysis and the formation of 5-thio-2-nitrobenzoate were measured spectrophotometrically using a UV-visible spectrometer (T-60, PG Instruments LTD., Leicestershire, UK) at 412 nm. AChE decomposes acetylcholine iodide and produces thiocholine. The interaction between thiocholine and DTNB results in 5-thio-2-nitrobenzoate production.[23,24]

Circular dichroism spectroscopy

To obtain insight into the potential effects of Fe_2O_3 NPs on the secondary structure of AChE, the circular dichroism spectroscopy (CD) spectra of AChE in the absence or presence of Fe_2O_3 NPs were measured in the far UV spectral region (200-250 nm) using a Jasco model spectropolarimeter at 25 °C. In this regard, different concentrations of Fe_2O_3 NPs (0-1000 nM) were added to 1.0 mL of 20 mM phosphate buffer solution (pH 7.4; 310 K) containing 2.0 mg/mL AChE. The prepared reaction mixtures were incubated for 5 minutes, and the far UV spectra of the samples were recorded from 200 nm to 250 nm.[25] Finally, CDNN software was used to calculate the percentage of changes in the secondary structural elements of the enzyme.

Surface plasmon resonance (SPR) measurements

The kinetic parameters of the AChE-Fe_2O_3 NPs interaction were investigated using SPR analysis at four different temperatures (298, 303, 310, and 313 K) to obtain the rate constants and affinity between AChE and Fe_2O_3 NPs. All the SPR analysis was carried out on a double-circuit channel MP-SPR Navi™ 210A device with gold chips (Bio Navis Ltd. Tampere, Finland) after immobilizing AChE on the carboxymethyl dextran (CMD) Au chip. In this regard, the CMD sensor chip was washed using a 10 mM acetate buffer solution (pH=4.5) and then appended to the SPR device. Subsequently, to establish a stable baseline,

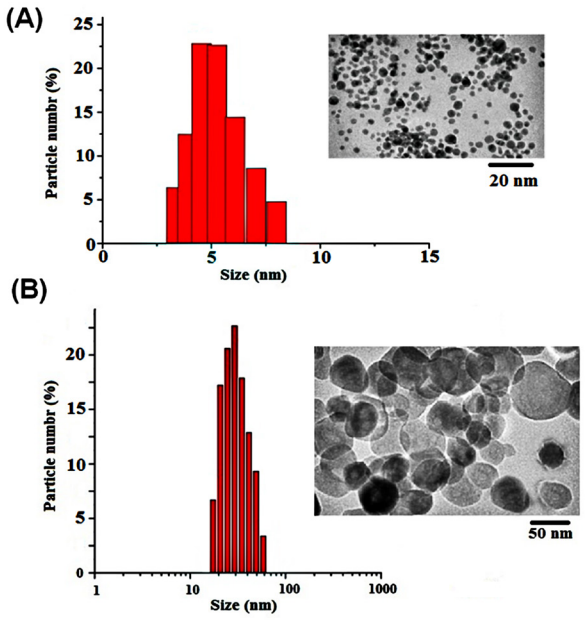

Fig. 1. DLS analysis of Fe_2O_3 NPs with 5 nm (A) and 50 nm (B) in size.

the chip surface was cleaned by injecting NaCl (2 M) and NaOH (0.1 M) into the apparatus for 30 min at a circuit rate of 30 µL/min. To activate the chip surface, a solution containing 0.05 M NHS and 0.2 M EDC was injected into the device for 7 min. Then, the prepared AChE solution was introduced into channel 1. Channel 2 was used as a reference channel. Finally, the immobilization process was completed by using 0.1 M ethanolamine-HCl (pH=8.5), which was injected into the Au chip surface to block the non-specific binding sites. In addition, to investigate the binding of Fe_2O_3 NPs to the immobilized AChE and the analysis of kinetic and thermodynamic parameters, additional concentrations of 5 nm Fe_2O_3 NPs (5, 100, 200, 400, and 800 nM) and 50 nm Fe_2O_3 NPs (0.5, 1, 2, 4, and 8 µM) were injected into channel 1. SPR Navi™ data viewer software and Trace Drawer™ were utilized for data analysis and the calculation of the interaction parameters, respectively.

Fluorescence spectroscopy

In this work, fluorescence spectroscopy was used to evaluate the conformational changes of AChE upon interaction with Fe_2O_3 NPs. For this purpose, the intrinsic fluorescence intensity of AChE was measured without and with various concentrations of Fe_2O_3 NPs (50-1000 nM) using a spectrofluorometer (Jasco, FP-750, Kyoto, Japan) with a 1.0 cm quartz cuvette. A fixed concentration of AChE (0.5 mg/mL) was incubated with different dosages of Fe_2O_3 NPs (50-1000 nM) for 5 minutes at 310 K in phosphate buffer solution (pH 7.4). Then, the enzyme was excited at 280 nm, and the emission spectra of the samples were recorded in the range of 300-500 nm. The slit width for the excitation and emission was 5 nm.[18]

Cell culture

To examine the potential effects of Fe_2O_3 NPs (5 nm and 50 nm) on the catalytic activity of AChE, HepG2 cell lines were cultivated in Williams-fetal bovine serum (Williams-FBS) media containing 10% FBS, 100 U/mL ampicillin, and 100 g/mL streptomycin. The cells were seeded per well of a 12-well culture plate and treated with a 2 µM concentration of Fe_2O_3 NPs. The treated and untreated control cells were incubated at 5% CO_2 in a humidified atmosphere of 95% air and 37 °C for 24 hours. Then, the inhibitory effect of Fe_2O_3 nanoparticles on AChE activity was evaluated by preparing cell lysate.[26] The experiments were repeated three times.

Statistical evaluation

All of the experimental data were analyzed by version 11 of SPSS software, and the expression of the data was done as mean ± standard deviation (SD). One-way variance (ANOVA) was used for the statistical analysis, followed by a multiple-range test using Dennett's approach. Differences at $P < 0.05$ were considered significant results.

Results and Discussion

Because it may regulate the cholinergic neurotransmitter in the synaptic cleft, AChE is a crucial enzyme for the nervous system's proper operation. Therefore, it is one of the main target enzymes in neural toxicity and progressive neurological disorders such as Alzheimer's. Fe_2O_3 NPs are applied in various scientific fields and different industries.[27] Applications of these NPs in different sizes have been rising in recent years. Despite the wide range of applications of NPs, particularly in medicine, their neurotoxicity poses challenges. Therefore, investigating the toxicity of NPs on various macromolecules, such as enzymes, proteins, and nucleic acids, is of great importance.

Effects of Fe_2O_3 NPs on catalytic activity of AChE

Due to their unique physiochemical properties, Fe_2O_3 NPs are widely used in many *in vivo* and *in vitro* research projects.[28] These materials are one of the most significant nanomaterials because of their extensive use in magnetic resonance imaging (MRI), ultrasound, optical imaging, X-ray imaging, drug delivery, gene delivery, etc.[29-31] Previous studies confirmed that this type of nanomaterials causes harsh oxidative damage in living systems.[32] By considering previous results and physiological signs of Fe_2O_3 NPs poisoning, the main objective of this study was to study the possible effects of Fe_2O_3 NPs in two different sizes, 5 nm and 50 nm, on the structure and catalytic activity of AChE. As shown in Fig. 2A, the Fe_2O_3 NPs with a 5 nm size inhibited the enzyme activity in a dose-dependent manner. AChE's catalytic activity was shown to be affected in two ways by 50 nm Fe_2O_3 NPs (Fig. 2B), and a continuous decrease of enzyme activity was observed with increasing concentrations of 5 nm Fe_2O_3 NPs. The results indicated that the enzyme's activity increased significantly with increasing the Fe_2O_3 NPs concentration (up to 60 nM). However, at higher concentrations than 60 nM, a reduction in enzyme activity was observed. It can be concluded that the particles of large size interfere with or compete at the catalytic site of the enzymes and inhibit their action. This suggests that competition with the substrate due to the hydrophobicity of the particle and NPs forming micelles with the microsomal membrane leads to a change in membrane integrity and, thus, enzyme inactivation.[33] In addition, with increasing the size of nanoparticles, their entrance into the active site of the enzymes reduces. Therefore, the conformation of the active site cannot be influenced by particles of large size.[34]

In addition, the inhibition type of the Fe_2O_3 NPs (5 and 50 nm) in the AChE action was evaluated. In this regard, AChE was incubated with different concentrations of 5 nm Fe_2O_3 NPs (0, 60, and 150 nM) and 50 nm Fe_2O_3 NPs (0, 700, and 1000 nM) and then the activity of the AChE was recorded spectrophotometrically. The results indicated that the catalytic activity of AChE was inhibited in the presence of increasing concentrations of Fe_2O_3 NPs through a mixed-type mechanism (Fig. 3). The calculated K_m and V_{max} values are listed in Table 1. As shown in Fig. 3A and B, increasing the 5 nm Fe_2O_3 NPs concentration mainly increased the K_m value from 1.81±0.09 mM for

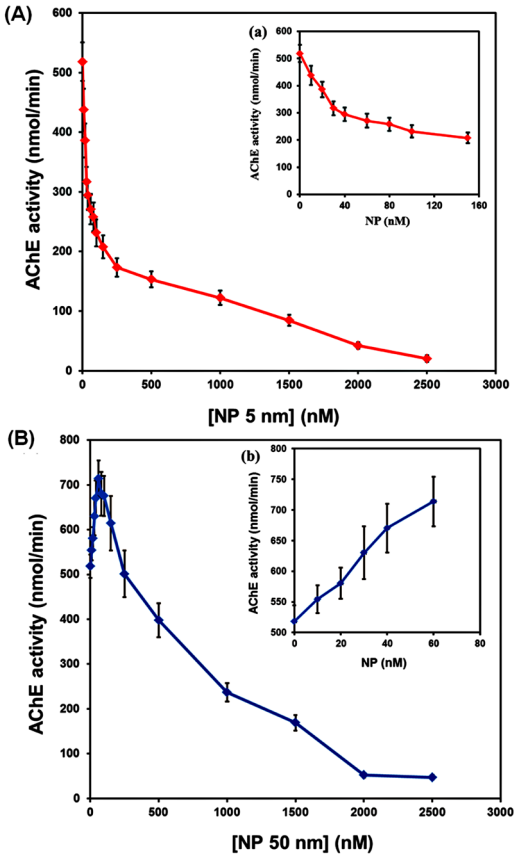

Fig. 2. AChE catalytic activity in the presence of Fe_2O_3 NPs of size 5 nm (A) and 50 nm (B) at 25 °C. Data was shown as mean±SD.

the free enzyme to 2.43±0.11 mM for the AChE-Fe_2O_3 NPs complex. Also, the V_{max} values decreased from 793.15±56.87 nmol/min for the free AChE to 364.28±23.65 nmol/min for the AChE upon interaction with Fe_2O_3 NPs. On the other hand, 50 nm Fe_2O_3 NPs caused a reduction in the K_m (from 1.81±0.09 mM to 1.31±0.05 mM) and V_{max} (from 793.15±56.87 nmol/min to 207.17±13.21 nmol/min) values of AChE (Fig. 3C and D). According to these results and based on the data reported in Table 1, it was concluded that Fe_2O_3 NPs (5 nm and 50 nm) are able to inhibit the catalytic activity of AChE through mixed mechanism of inhibition.[35] According to the results 5 nm NPs could bind to the free enzyme more than enzyme-substrate complex that refer to a competitive-noncompetitive inhibition while the 50 nm NPs prefer to bind to the enzyme-substrate complex (noncompetitive-uncompetitive type of inhibition).

Table 1. The calculated apparent K_m and V_{max} values for AChE in the presence of Fe_2O_3 NPs

Ligand	[NPs] (nM)	K_m (nM)	V_{max} (nmol/min)
Fe_2O_3 $NPs_{(5\ nm)}$	0	1.81±0.09	793.15±56.87
	60	2.11±0.11	499.27±32.72
	150	2.43±0.11	364.28±23.65
Fe_2O_3 $NPs_{(50\ nm)}$	0	1.81±0.09	793.15±56.87
	700	1.60±0.07	348.09±21.47
	1000	1.31±0.05	207.17±13.21

Data was represented as mean ± SD.

Fluorescence spectroscopy studies

Fluorescence spectroscopy is one of the most simple, sensitive, and inexpensive methods for evaluating the interactions between macromolecules and ligands, such as protein-ligand interactions. Three different aromatic amino acid residues, including tyrosine (Tyr), tryptophan (Trp), and phenylalanine (Phe), exist in the AChE structure.[36] The intrinsic fluorescence intensity of AChE comes from these residues, which are very sensitive to rearrangements in the polarity of their environment.[18] In this work, the effect of additional concentrations of Fe_2O_3 NPs on the emission intensity of AChE was investigated. The maximal emission spectrum of the AChE was observed at 360 nm, a characteristic of Trp residues in a slightly hydrophilic environment. The results showed that Fe_2O_3 NPs can reduce an enzyme's intrinsic emission by changing its conformation and the polar micro-region of aromatic amino acids (Fig. 4). The fluorescence quenching effects of AChE in the presence of Fe_2O_3 NPs depict a less compact structure due to increased distances between the fluorophore molecules as well as their more significant interactions with the hydrophilic environment that result in fluorescence quenching.[36] The study also showed no shift in the position of the Trp residues, which means that although the inhibitor interacted very closely with AChE to quench fluorescence, the secondary structures of the enzyme may not have been altered.[37] It is suggested that a new non-fluorescent complex was formed between AChE and Fe_2O_3 NPs. The tertiary structure of AChE, in particular the substrate entrance gate of the active site, may be impacted by these particles, which inhibits the enzyme's catalytic activity.

CD spectroscopy studies

CD spectroscopy is one of the acceptable methods for monitoring the conformational and structural alternations in the secondary structure of different macromolecules, such as proteins induced via binding to specific molecular substances.[38] To look into potential impacts on the secondary structure of AChE, a specific concentration (2 mg/mL) of AChE was incubated with various concentrations of Fe_2O_3 NPs (50–1000 nM) for 3 min, and then, the CD spectra of the samples were recorded in the range of 200-250 nm. In general, the CD spectra of AChE show two main negative bonds, which are located at 208 nm and 222 nm.[39] These negative bands are related to $\pi \longrightarrow \pi^*$ and $n \longrightarrow \pi^*$ transitions of amide groups in α-helical structure, respectively. Also, a negative band around 217 nm corresponds to the β-sheets.[18] Fig. 5 shows the CD spectra of AChE upon interaction with Fe_2O_3 NPs. As shown in this figure, after incubating with

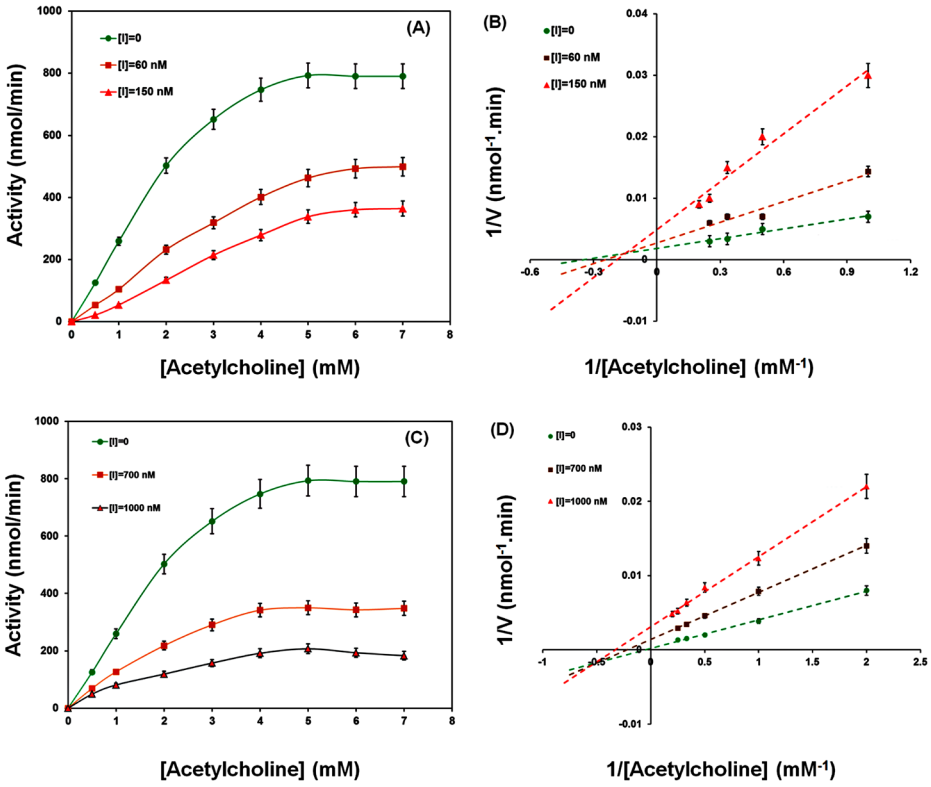

Fig. 3. Michaelis-Menten and Lineweaver-Burk plots of AChE with and without various concentrations of Fe_2O_3 NPs with 5 nm (A and B) and 50 nm (C and D) in size.

Fe_2O_3 NPs, the α-helix and β-sheets contents decreased in the AChE structure. According to Table 2, the native AChE showed a preponderance of 30.1% α-helix, 21.9% β-sheets, 15.2 % β-turn, and 32.8% unordered structures. However, the percentages of these elements changed upon interaction with Fe_2O_3 NPs of different sizes. The results indicated that the contents of α-helix were decreased to 18.3% and 10.3% in the presence of Fe_2O_3 NPs with 5 nm and 50 nm (1000 nM), respectively. In addition, Fe_2O_3 NPs with 5 nm and 50 nm reduced the percentages of β-sheets to 13.8% and 8.5%, respectively. So, these results showed that Fe_2O_3 NPs can reduce the stability of AChE by decreasing the α-helical structures that refer to the denaturing of proteins in the presence of NPs. The outcomes indicated the alterations in conformation and secondary structure of AChE in the presence of Fe_2O_3 NPs with a 50 nm size were higher than those of 5 nm Fe_2O_3 NPs. Due to the existence of the active site of AChE between α-helix and β-sheet domains, it can be concluded that the catalytic activity of the enzyme can be influenced

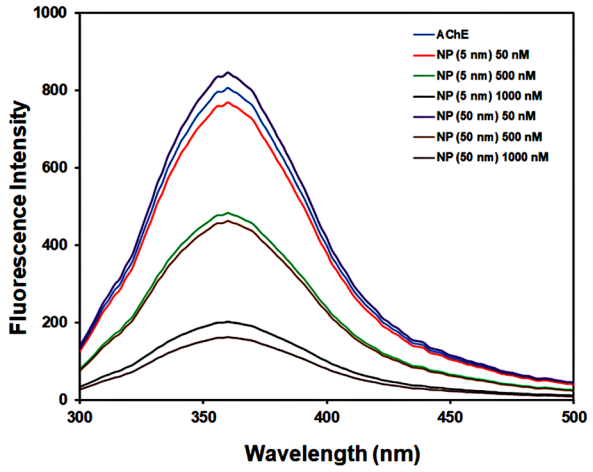

Fig. 4. Fluorescence spectra of AChE without and with different concentrations (50, 500, and 1000 nM) of Fe_2O_3 NPs (5 nm, and 50 nm).

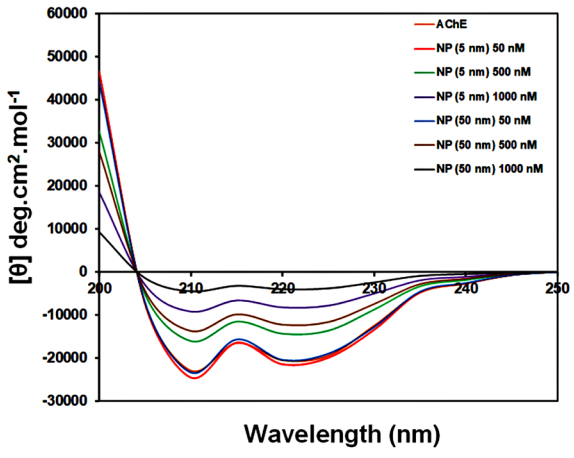

Fig. 5. CD spectra of AChE in the absence and presence of additional concentrations (50, 500, and 1000 nM) of Fe_2O_3 NPs.

Table 2. Content of secondary structure elements of AChE upon interaction with Fe2O3 NPs at room temperature

	[NPs] (nM)	Secondary structure content in AChE (%)			
		α-helix	β-sheet	β-turns	Random coil
Fe_2O_3 $NPs_{(5\ nm)}$	0	30.1	21.9	15.2	32.8
	50	31.8	22.3	15.9	30.0
	500	24.6	20.1	18.8	36.5
	1000	18.3	13.8	22.1	45.8
Fe_2O_3 $NPs_{(50\ nm)}$	50	30.2	21.7	14.9	33.2
	500	22.6	18.9	21.5	37
	1000	10.3	8.5	12.9	68.3

by any changes in their conformations and contents.[18] The structure of the active site may also be impacted by AChE's secondary conformational changes, which impact the substrate entrance gate and enzyme activity.[40] Therefore, it is suggested that the active site rearrangement caused by Fe_2O_3 NPs may eventually result in substrate traffic at the entrance gate.

SPR results

The kinetic parameters of the interaction of Fe_2O_3 NPs with immobilized AChE were assessed using the SPR technique. These parameters reveal the affinity between a ligand and a macromolecule. To this end, different concentrations of Fe_2O_3 NPs were injected into the chip surface, and then the SPR signals were recorded. Fig. 6 shows the SPR sensorgram of the binding of AChE with Fe_2O_3 NPs at 298K (the SPR sensorgrams at 303, 310, and 313 K are not shown). It is clear that with increasing the concentration of Fe_2O_3 NPs the binding signal gradually increased, too. The equilibrium constant (K_D) values were calculated, and the findings are summarized in Table 3. According to this table, the low values of K_D indicate a high affinity between ligands and AChE.[41] Additionally, the findings showed that the K_D values increased as the temperature rose, supporting that the affinity between AChE and Fe_2O_3 NPs and the reaction rate decreased with rising temperature.[42]

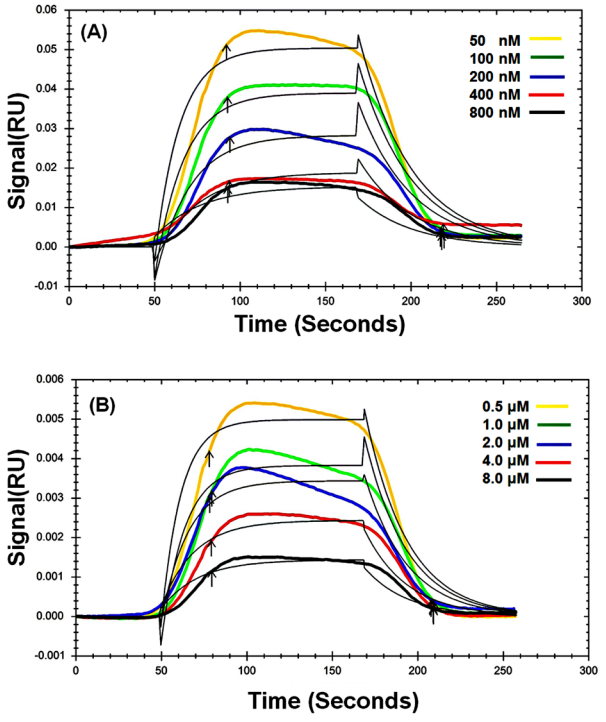

Fig. 6. Dose-response sensorgrams of AChE in the presence of Fe_2O_3 NPs with 5 nm (A) and 50 nm (B) in size at 298 K.

Thermodynamic analysis

It has been reported that various acting forces, such as hydrogen bonds, electrostatic forces, Vander Waals forces, and hydrophobic interactions, play a critical role in the complex formation between a ligand and a macromolecule.[38,43] In the present work, the thermodynamic parameters were calculated using equations 1 and 2.

$$\ln K_D = -\frac{\Delta H}{RT} + \frac{\Delta S}{R} \quad (1)$$

$$\Delta G = \Delta H - T\Delta S \quad (2)$$

Here, R (8.314 J/mol/K) is the universal gas constant and T denotes the absolute temperature, respectively.

The plot of $\ln K_D$ against 1/T (Van't Hoff plot) was constructed and then the slope and the intercept of the plot was used for the calculation of ΔH and ΔS, respectively (Fig. 7). The calculated values are reported in Table 3. Based on these data, it can be concluded that Fe_2O_3 NPs bind AChE non-spontaneously (ΔG>0). Also, the positive values of ΔH means that the system has gotten energy from the surroundings in the form of heat. In addition, the reaction was an endothermic since the products have a greater energy level than the reactants and the net heat was absorbed. A positive ΔH and negative ΔS cause a positive ΔG so the reaction is not spontaneous.

AChE activity of HepG2 cells

In this work, HepG2 cells were utilized as a model to investigate the impact of Fe_2O_3 NPs on AChE catalytic activity inside the cells. For this purpose, the prepared cell lysates were used to assess the catalytic activity of AChE. The findings are shown in Fig. 8. It can be seen from this figure that Fe_2O_3 NPs caused a decrease in AChE activity. However, the inhibitory effect of Fe_2O_3 NPs with

Table 3. Equilibrium constants (K_D) for binding of Fe_2O_3 NPs (5 nm and 50 nm) to AChE at different temperatures

Sample	T (K)	K_D (M)	ΔH (kJ/mol)	ΔS (kJ/mol)	ΔG (kJ/mol/ k)
Fe_2O_3 $NPs_{(5\ nm)}$	298	2.8×10^{-8}	14.14	-0.097	43.09
	303	3.1×10^{-8}			43.57
	310	3.5×10^{-8}			44.26
	313	3.7×10^{-8}			44.55
Fe_2O_3 $NPs_{(50\ nm)}$	298	6.4×10^{-4}	4.39	-0.046	18.20
	303	6.7×10^{-4}			18.43
	310	6.9×10^{-4}			18.76
	313	7.0×10^{-4}			18.90

a 5 nm size (65 %) was significantly higher than that of a 50 nm size (20%). Therefore, it can be concluded that Fe_2O_3 NPs inhibit the catalytic activity of AChE in a size-dependent manner. Based on these results, nanoparticles with a smaller size can easily cross the blood-brain barrier, interact with various neurological targets such as AChE, and cause neurotoxic effects.[44] According to this study, due to their interaction with AChE, Fe_2O_3 NPs (of various sizes) may not be safe or even be neurotoxic. However, the small particles have a more significant neurotoxic effect on the native structure and catalytic activity of AChE.[44,45]

Conclusion

In this work, the inhibitory effects of Fe_2O_3 NPs (with two different sizes, 5 nm, and 50 nm) on the catalytic activity of AChE were investigated, and the obtained results indicated that Fe_2O_3 NPs can inhibit AChE activity in a dose-dependent manner. The results confirmed the inhibitory effect of 5 nm Fe_2O_3 NPs on AChE activity via mixed mechanism. However, it was observed that the AChE activity was increased in the presence of 50 nm Fe_2O_3 NPs (up to 60 nM) and then decreased. Also, conformational studies were performed using fluorescence and CD spectroscopy analysis. The results suggested that Fe_2O_3 NPs could change the secondary and tertiary structures of the enzyme by reducing the amount of α-helix and β-sheet, leading to the unfolding of the enzyme structure. According to the results, the conformational changes of the enzyme in the presence of 50 nm Fe_2O_3 NPs were higher than those of 5 nm Fe_2O_3 NPs. On the other hand, the interaction between AChE and Fe_2O_3 NPs was studied using the SPR method, and the results indicated that the K_D values increased with rising temperature, suggesting a reduction in the affinity of AChE towards Fe_2O_3 NPs. Thermodynamic studies revealed that the AChE/Fe_2O_3 NPs complex was formed through a nonspontaneous process. In addition, the effect of Fe_2O_3 NPs on AChE catalytic activity was evaluated in HepG2 cell lines, and the obtained results showed that the inhibitory effect of Fe_2O_3 NPs with a 5 nm size was significantly higher than that of a 50 nm size, possibly due to increased surface area to volume ratio. This study provided new insights into the impact of Fe_2O_3 NPs on the function and structure of AChE, and a novel mechanism of Fe_2O_3 NPs poisoning in the dysfunction of the cholinergic system. Considering the increasing application of NPs in different fields and specific features of NPs such as high reactivity, penetration through the blood-brain barrier, and oxidative damage, our results provide strong reasons why the application of NPs should be limited in all aspects of life. It is valuable

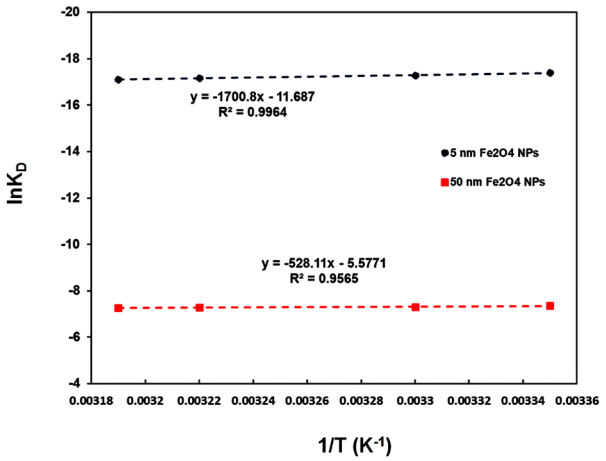

Fig. 7. Van't Hoff curves for the binding of Fe_2O_3 NPs with 5 nm (A) and 50 nm (B) in size to AChE.

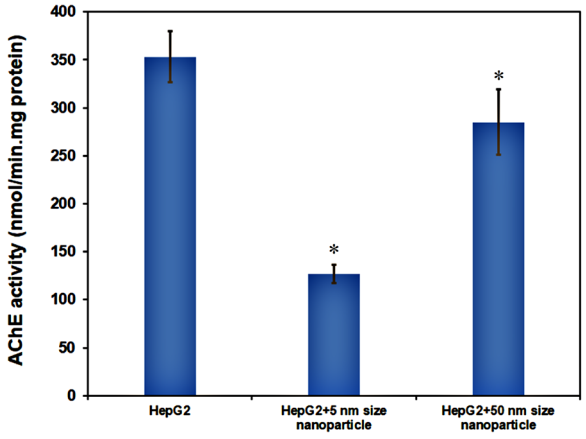

Fig. 8. AChE activity assessment in HepG2 cell lines in the absence and presence of Fe_2O_3 NPs. Data was shown as mean±SD and star symbols show significant difference (P<0.05) in comparison with the control (without NPs).

Research Highlights

What is the current knowledge?

√ During the last decade, nanotechnology has had extensive applications as nanomedicine in the medical field.

√ Hence, it is essential to establish the toxicity, safety, and risks involved in the use of nanoparticles.

What is new here?

√ The effect of Fe2O3 NPs on AChE activity depends on the size of the nanoparticles.

√ The Fe_2O_3 NPs nanoparticles in small sizes inhibit enzyme activity, but in larger sizes, they show a dual effect on enzyme activity.

√ The Fe_2O_3 NPs inhibit the enzyme activity in vivo.

to notice that the results of this study could help extend the knowledge of utilizing Fe_2O_3 NPs for poisoning in the neural system.

Authors' Contribution

Conceptualization: Leila Sadeghi, Samaneh Rashtbari, Zahra Hassanpour Aydinlou.
Data curation: Leila Sadeghi, Samaneh Rashtbari.
Investigation: Samaneh Rashtbari, Zahra Hassanpour Aydinlou.
Project administration: Leila Sadeghi.
Supervision: Leila Sadeghi.
Validation: Leila Sadeghi, Samaneh Rashtbari.
Visualization: Leila Sadeghi, Samaneh Rashtbari.
Writing–original draft: Samaneh Rashtbari, Zahra Hassanpour Aydinlou.
Writing–review editing: Leila Sadeghi.

Competing Interests

We wish to confirm that there are no known conflicts of interest associated with this publication.

Ethical Statement

None to be stated.

Funding

None to be stated.

References

1. Srivastava V, Gusain D, Sharma YC. Critical review on the toxicity of some widely used engineered nanoparticles. *Ind Eng Chem Res* **2015**; 54: 6209-33. https://doi.org/10.1021/acs.iecr.5b01610
2. Mirzajani F, Motevalli SM, Jabbari S, Siadat SOR, Sefidbakht Y. Recombinant acetylcholinesterase purification and its interaction with silver nanoparticle. *Protein Expr Purif* **2017**; 136: 58-65. https://doi.org/10.1016/j.pep.2017.05.007
3. Rashtbari S, Dehghan G, Khataee S, Amini M, Khataee A. Dual enzymes-mimic activity of nanolayered manganese-calcium oxide for fluorometric determination of metformin. *Chemosphere* **2022**; 291: 133063. https://doi.org/10.1016/j.chemosphere.2021.133063
4. Rashtbari S, Dehghan G, Amini M, Khorram S, Khataee A. A sensitive colori/fluorimetric nanoprobe for detection of polyphenols using peroxidase-mimic plasma-modified MoO3 nanoparticles. *Chemosphere* **2022**; 295: 133747. https://doi.org/10.1016/j.chemosphere.2022.133747
5. Dietrich J, Enke A, Wilharm N, Konieczny R, Lotnyk A, Anders A, *et al.* Energetic Electron-Assisted Synthesis of Tailored Magnetite (Fe3O4) and Maghemite (γ– Fe2O3) Nanoparticles: Structure and Magnetic Properties. *Nanomaterials* **2023**; 13: 786.
6. Mahmoudi M, Shokrgozar MA, Sardari S, Moghadam MK, Vali H, Laurent S, *et al.* Irreversible changes in protein conformation due to interaction with superparamagnetic iron oxide nanoparticles. *Nanoscale* **2011**; 3: 1127-38. https://doi.org/10.1039/c0nr00733a
7. Dulińska-Litewka J, Łazarczyk A, Hałubiec P, Szafrański O, Karnas K, Karewicz A. Superparamagnetic iron oxide nanoparticles—Current and prospective medical applications. *Materials* **2019**; 12: 617. https://doi.org/10.3390/ma12040617
8. Nguyen MD, Tran H-V, Xu S, Lee TR. Fe3O4 nanoparticles: structures, synthesis, magnetic properties, surface functionalization, and emerging applications. *Appl Sci* **2021**; 11: 11301.
9. Srinoi P, Chen Y-T, Vittur V, Marquez MD, Lee TR. Bimetallic nanoparticles: enhanced magnetic and optical properties for emerging biological applications. *Appl Sci* **2018**; 8: 1106.
10. Wu K, Saha R, Su D, Krishna VD, Liu J, Cheeran MC-J, *et al.* Magnetic-nanosensor-based virus and pathogen detection strategies before and during COVID-19. *ACS Appl Nano Mater* **2020**; 3: 9560-80. https://doi.org/10.1021/acsanm.0c02048
11. Rashtbari S, Dehghan G, Amini M. An ultrasensitive label-free colorimetric biosensor for the detection of glucose based on glucose oxidase-like activity of nanolayered manganese-calcium oxide. *Anal Chim Acta* **2020**; 1110: 98-108. https://doi.org/10.1016/j.aca.2020.03.021
12. Rashtbari S, Dehghan G, Khorram S, Amini M, Khataee A, Yoon Y. Plasma modified Co3O4 nanoparticles for catalytic degradation process through enhanced peroxidase-like activity. *J Ind Eng Chem* **2023**; 121: 114-123. https://doi.org/10.1016/j.jiec.2023.01.015
13. Wu Z, Zhang B, Yan B. Regulation of enzyme activity through interactions with nanoparticles. *Int J Mol Sci* **2009**; 10: 4198-209. https://doi.org/10.3390/ijms10104198
14. Radman M. Dysfunction and toxicity of damaged proteins in the etiology of aging and age-related degenerative and malignant diseases. *Croat Med J* **2020**; 61: 159-66. https://doi.org/10.3325/cmj.2020.61.159
15. Aletaha N, Dehghan G, Sadeghi L, Rashtbari S, Khataee A. Binding mechanism of perphenazine/thioridazine with acetylcholinesterase: Spectroscopic surface plasmon resonance and molecular docking based analysis. *J Mol Liq* **2023**; 377: 121547. https://doi.org/10.1016/j.molliq.2023.121547
16. Campanha HM, Carvalho F, Schlosser PM. Active and peripheral anionic sites of acetylcholinesterase have differential modulation effects on cell proliferation, adhesion and neuritogenesis in the NG108-15 cell line. *Toxicol Lett* **2014**; 230: 122-31. https://doi.org/10.1016/j.toxlet.2014.03.012
17. Assis CRD, Linhares AG, Oliveira VM, França RCP, Santos JF, Carvalho E, *et al.* Effect of ions on the activity of brain acetylcholinesterase from tropical fish. *Journal of Coastal Life Medicine* **2015**; 3: 505-14. http://dx.doi.org/10.12980/JCLM.3.2015J5-11
18. Yekta R, Sadeghi L, Dehghan G. The inefficacy of donepezil on glycated-AChE inhibition: Binding affinity, complex stability and mechanism. *Int J Biol Macromol* **2020**; 160: 35-46. https://doi.org/10.1016/j.ijbiomac.2020.05.177
19. Colovic MB, Krstic DZ, Lazarevic-Pasti TD, Bondzic AM, Vasic VM. Acetylcholinesterase inhibitors: pharmacology and toxicology. *Curr Neuropharmacol* **2013**; 11: 315-35. https://doi.org/10.2174/1570159X11311030006
20. Hayden KM, Norton MC, Darcey D, Østbye T, Zandi PP, Breitner J, *et al.* Occupational exposure to pesticides increases the risk of incident AD: the Cache County study. *Neurology* **2010**; 74: 1524-30. https://doi.org/10.1212/WNL.0b013e3181dd4423
21. Askri D, Cunin V, Ouni S, Béal D, Rachidi W, Sakly M, *et al.* Effects of iron oxide nanoparticles (γ-Fe2O3) on liver, lung and brain proteomes following sub-acute intranasal exposure: A new toxicological assessment in rat model using iTRAQ-based quantitative proteomics. *Int J Mol Sci* **2019**; 20: 5186. https://doi.org/10.3390%2Fijms20205186
22. Ellman GL, Courtney KD, Andres Jr V, Featherstone RM. A new and rapid colorimetric determination of acetylcholinesterase activity.

Biochem Pharmacol **1961**; 7: 88-95. https://doi.org/10.1016/0006-2952(61)90145-9
23. Worek F, Eyer P, Thiermann H. Determination of acetylcholinesterase activity by the Ellman assay: a versatile tool for in vitro research on medical countermeasures against organophosphate poisoning. *Drug Test Anal* **2012**; 4: 282-91. https://doi.org/10.1002/dta.337
24. Yousefi Babadi V, Sadeghi L, Shirani K, Malekirad AA, Rezaei M. The toxic effect of manganese on the acetylcholinesterase activity in rat brains. *J Toxicol* **2014**; 2014: 946372. https://doi.org/10.1155/2014/946372
25. Patil DN, Patil SA, Sistla S, Jadhav JP. Comparative biophysical characterization: A screening tool for acetylcholinesterase inhibitors. *PLoS One* **2019**; 14: e0215291. https://doi.org/10.1371/journal.pone.0215291
26. Pérez-Aguilar B, Vidal CJ, Palomec G, García-Dolores F, Gutiérrez-Ruiz MC, Bucio L, *et al.* Acetylcholinesterase is associated with a decrease in cell proliferation of hepatocellular carcinoma cells. *Biochim Biophys Acta Mol Basis Dis* **2015**; 1852: 1380-7. https://doi.org/10.1016/j.bbadis.2015.04.003
27. Van Nhan L, Ma C, Rui Y, Cao W, Deng Y, Liu L, *et al.* The effects of Fe2O3 nanoparticles on physiology and insecticide activity in non-transgenic and Bt-transgenic cotton. *Front Plant Sci* **2016**; 6: 1263. https://doi.org/10.3389/fpls.2015.01263
28. Sun C, Lee JS, Zhang M. Magnetic nanoparticles in MR imaging and drug delivery. *Adv Drug Deliv Rev* **2008**; 60: 1252-65. https://doi.org/10.1016/j.addr.2008.03.018
29. Hemalatha T, Prabu P, Gunadharini DN, Gowthaman MK. Fabrication and characterization of dual acting oleyl chitosan functionalised iron oxide/gold hybrid nanoparticles for MRI and CT imaging. *Int J Biol Macromol* **2018**; 112: 250-7. https://doi.org/10.1016/j.ijbiomac.2018.01.159
30. Unsoy G, Yalcin S, Khodadust R, Gunduz G, Gunduz U. Synthesis optimization and characterization of chitosan-coated iron oxide nanoparticles produced for biomedical applications. *J Nanopart Res* **2012**; 14: 1-13. https://doi.org/10.1007/s11051-012-0964-8
31. Al-Hakkani MF, Gouda GA, Hassan SH. A review of green methods for phyto-fabrication of hematite (α-Fe2O3) nanoparticles and their characterization, properties, and applications. *Heliyon* **2021**; 7: e05806. https://doi.org/10.1016/j.heliyon.2020.e05806
32. Sadeghi L, Tanwir F, Babadi VY. In vitro toxicity of iron oxide nanoparticle: Oxidative damages on Hep G2 cells. *Exp Toxicol Pathol* **2015**; 67: 197-203. https://doi.org/10.1016/j.etp.2014.11.010
33. Fröhlich E, Kueznik T, Samberger C, Roblegg E, Wrighton C, Pieber TR. Size-dependent effects of nanoparticles on the activity of cytochrome P450 isoenzymes. *Toxicol Appl Pharmacol* **2010**; 242: 326-32. https://doi.org/10.1016/j.taap.2009.11.002
34. Chen W-Q, Wu W-J, Yu Y-Q, Liu Y, Jiang F-L. New Insights on the Size-Dependent Inhibition of Enzymes by Gold Nanoparticles. *Langmuir* **2023**; 39: 9595-603. https://doi.org/10.1021/acs.langmuir.3c01367
35. Agarwal PK. Enzymes: An integrated view of structure, dynamics and function. *Microbial cell factories* **2006**; 5: 1-12. https://doi.org/10.1186/1475-2859-5-2
36. Asen ND, Okagu OD, Udenigwe CC, Aluko RE. In vitro inhibition of acetylcholinesterase activity by yellow field pea (Pisum sativum) protein-derived peptides as revealed by kinetics and molecular docking. *Front Nutr* **2022**; 9: 1021893. https://doi.org/10.3389/fnut.2022.1021893
37. Malta SM, Batista LL, Silva HCG, Franco RR, Silva MH, Rodrigues TS, *et al.* Identification of bioactive peptides from a Brazilian kefir sample, and their anti-Alzheimer potential in Drosophila melanogaster. *Sci Rep* **2022**; 12: 11065. https://doi.org/10.1038/s41598-022-15297-1
38. Rashtbari S, Dehghan G, Yekta R, Jouyban A. Investigation of the binding mechanism and inhibition of bovine liver catalase by quercetin: Multi-spectroscopic and computational study. *Bioimpacts* **2017**; 7: 147. https://doi.org/10.15171/bi.2017.18
39. Xiang J, Yu C, Yang F, Yang L, Ding H. Conformation-activity studies on the interaction of berberine with acetylcholinesterase: Physical chemistry approach. *Prog Nat Sci* **2009**; 19: 1721-5. https://doi.org/10.1016/j.pnsc.2009.07.010
40. Colletier JP, Fournier D, Greenblatt HM, Stojan J, Sussman JL, Zaccai G, *et al.* Structural insights into substrate traffic and inhibition in acetylcholinesterase. *EMBO J* **2006**; 25: 2746-56. https://doi.org/10.1038/sj.emboj.7601175
41. Rashtbari S, Dehghan G, Sadeghi L, Sareminia L, Iranshahy M, Iranshahi M, *et al.* Interaction of bovine serum albumin with ellagic acid and urolithins A and B: Insights from surface plasmon resonance, fluorescence, and molecular docking techniques. *Food Chem Toxicol* **2022**; 162: 112913. https://doi.org/10.1016/j.fct.2022.112913
42. Khataee S, Dehghan G, Yekta R, Rashtbari S, Maleki S, Khataee A. The protective effect of natural phenolic compound on the functional and structural responses of inhibited catalase by a common azo food dye. *Food Chem Toxicol* **2022**; 160: 112801. https://doi.org/10.1016/j.fct.2021.112801
43. Rashtbari S, Dehghan G, Yekta R, Jouyban A, Iranshahi M. Effects of resveratrol on the structure and catalytic function of bovine liver catalase (BLC): spectroscopic and theoretical studies. *Adv Pharm Bull* **2017**; 7: 349. https://doi.org/10.15171/apb.2017.042
44. Khatoon A, Khan F, Ahmad N, Shaikh S, Rizvi SMD, Shakil S, *et al.* Silver nanoparticles from leaf extract of Mentha piperita: eco-friendly synthesis and effect on acetylcholinesterase activity. *Life Sci* **2018**; 209: 430-4. https://doi.org/10.1016/j.lfs.2018.08.046
45. Cabaleiro-Lago C, Lundqvist M. The effect of nanoparticles on the structure and enzymatic activity of human carbonic anhydrase I and II. *Molecules* **2020**; 25: 4405. https://doi.org/10.3390/molecules25194405